Electronic Supplementary Information

Ultrasmall PdPtCo Trimetallic Nanorings with Enriched Low-Coordinated Edge Sites and Optimized Compositions for Effective Oxygen Reduction Electrocatalysis

Chao Zhen,[a] Zixi Lyu,[a] Kai Liu,[a] Xuejiao Chen,[a,] Yu Sun,[a] Xinyan Liao,[a] and Shuifen Xie[a,]**

[a]Xiamen Key Laboratory of Optoelectronic Materials and Advanced Manufacturing, College of Materials Science and Engineering, Huaqiao University, Xiamen 361021, China

*Correspondence author emails: sfxie@hqu.edu.cn; xjchen@hqu.edu.cn

Part I: Experimental section

Materials

Palladium(II) acetylacetone [$Pd(acac)_2$, ≥ 99.0%] and platinum(II) acetylacetone [$Pt(acac)_2$, ≥ 99.0%] were purchased from Kunming Institute of Precious Metals. Potassium bromide (KBr, ≥ 99.0%), N, N-dimethylformamide (DMF, 99.9%) and ethanol (C_2H_5OH, ≥ 99.7%) were purchased from Xilong Chemical Co. Ltd. (China). Cobalt(II) acetylacetonate [$Co(acac)_2$, 95%], polyvinylpyrrolidone (PVP, Mw~58000), and citrate acid (CA, ≥ 99.5%) were purchased from Sigma-Aldrich. Hexacarbonyltungsten [$W(CO)_6$, 97%] was purchased from Alfa Aesar. Potassium hydroxide (KOH, 95%) was purchased from Macklin. Commercial Pt/C (20 wt%) catalyst was purchased from Johnson Matthey, oxygen gas (O_2, 99.999%) and carbon monoxide gas (CO, 99.999%) were provided by Linde Industrial Gases. All chemicals were used without further purification.

Preparation of 2D multimetallic ultrathin nanostructures and electrocatalysts

Synthesis of PdPtCo trimetallic ultrathin nanorings (NRs). In a typical synthesis of $Pd_{55}Pt_{18}Co_{27}$ NRs, 90 mg CA, 20 mg KBr, 30 mg PVP, 16 mg $Pd(acac)_2$, 8 mg $Pt(acac)_2$, 15.4 mg $Co(acac)_2$ were added into a 25 mL glass vial containing 10 mL DMF. The mixture was first stirred at room temperature for 1 h followed by adding 100 mg $W(CO)_6$ into the vial. Then, the vial was sealed and stirred in an 80 ^oC oil bath for 3h and then ramped up to 150 ^oC and kept at this temperature for another 3 h. After cooling down to the room temperature, the products were collected by centrifugation and washing with anhydrous ethanol for four times. To synthesize the $Pd_{76}Pt_{19}Co_5$ and $Pd_{37}Pt_{10}Co_{53}$ ultrathin NRs, the above standard procedure was employed and the addition of $Co(acac)_2$ was adjusted to 7.7 mg and 30.8 mg, respectively.

Synthesis of PdPtCo and PdPt multimetallic ultrathin nanosheets (NSs). To fabricate the $Pd_{63}Pt_{16}Co_{21}$ NSs, all the conditions were kept following the standard procedure but the addition of $W(CO)_6$ was adjusted to 200 mg. The $Pd_{74}Pt_{26}$ NSs were synthesized with the standard method without the addition of $Co(acac)_2$.

Preparation of 2D multimetallic ultrathin NRs and NSs modified working electrode. For the electrocatalysis tests, the as-synthesized 2D multimetallic NRs and NSs were first loaded on the carbon support (Vulcan XC-72) with a 20 wt% loading of Pd and Pt and then casted on

a glassy carbon rotating disk electrode (GC-RDE, 0.196 cm^2). Specifically, the multimetallic NRs and NSs were dispersed in a mixture containing XC-72 (2.0 mg), ethanol (2.0 mL), and Nafion (10 μL, 0.5% ethanol solution) followed by fully sonication and stirring to form the homogeneous catalyst ink. Then, 8 μL the as-prepared ink (Pd+Pt = 2 μg) was carefully transferred and casted on the GC-RDE through a pipette. At last, the loaded electrode was dried at room temperature.

Characterization

Transmission electron microscopy (TEM), high-resolution TEM (HRTEM), high-angle annular dark field scanning TEM (HAADF-STEM), energy-dispersive X-ray spectroscopy (EDS) elemental mapping were conducted on a FEI Talos F200s with an accelerating voltage of 200 kV. Low-magnification TEM was collected using a JEOL JEM 2100 operating at 100 kV. All the samples were prepared by dropping the diluted ethanol suspension of samples on the carbon-coated copper TEM grids. Powder X-ray diffraction (PXRD) pattern was performed on a Rigaku Smart Lab with a Cu Kα X-ray source (λ = 1.5418 Å) at 30 mA and 40 kV. The concentration of catalyst was determined by inductively coupled plasma mass spectrometry (ICP-MS) (Agilent 7800). XPS was conducted on the Thermo ESCALAB 250XI. UPS was recorded on the PHI5000 VersaProbe III. Electrochemical measurements were carried out on a CHI 660E workstation (Shanghai Chenhua Co., Ltd., China) and a rotating electrode controller (Pine Research Instrumentation, AFMSRCE).

Electrochemical measurements

Electrochemical experiments were carried out with a three-electrode system consisted of a working electrode, a Pt mesh electrode, and a saturated calomel electrode (SCE). All potentials were reported with reference to the reversible hydrogen electrode (RHE) by the following equation, *i.e.*, $E_{RHE} = E_{SCE} + 0.059\ pH + 0.241\ V$. CV cycles were recorded at a scan rate of 50 mV s^{-1} from -0.25 to 0.85 V (vs. SCE) in N_2 saturated 0.1 M $HClO_4$. CO stripping voltammetry was performed to evaluate the electrochemically active surface areas (ECSAs) of the catalysts. The electrodes were placed in the CO-saturated 0.1M $HClO_4$ for 20 min, and then transferred to a fresh N_2-saturated 0.1M $HClO_4$ and swept from -0.25 to 0.95 V (vs. SCE) with

a scan rate of 20 mV·s^{-1}. Linear sweep voltammetry (LSV) of the above electrodes in the O_2-saturated 0.1 M KOH was employed to record the ORR polarization curves with a scan rate of 10 mV·s^{-1} and a rotation rate of 1600 rpm. Tafel curves were converted from these ORR polarization curves. Other polarization curves measured with different rotating rates spanning from 800-2400 rpm were also recorded for the fitting of Koutecký-Levich (K-L) correlation. All the LSV curves were measured under 90% *iR*-compensation condition.

The electron transfer numbers (n) per oxygen molecule and kinetic current densities (j_k) of the above electrodes were calculated through fitting the Koutecký-Levich (K-L) correlation (Eq. 1, 2).

$$\frac{1}{j} = \frac{1}{j_k} + \frac{1}{j_l} \qquad \text{Eq. 1}$$

$$j_l = 0.62nFD^{2/3}v^{-1/6}C\omega^{1/2} \qquad \text{Eq. 2}$$

Here, j is the measured current density, j_k and j_l are the kinetic and diffusion-limiting current densities, respectively. ω is the angular velocity of rotation ($\omega = 2\pi f$, where f is the RDE rotation rate in the unit of rpm), F is Faraday constant (96485 C·mol^{-1}), D is the diffusion coefficient of O_2 in the 0.1 M KOH (1.93×10^{-5} cm^2·s^{-1}), v is the kinematic viscosity (1.01×10^{-2} cm^2·s^{-1}), and C is the bulk concentration of O_2 in the electrolyte (1.26×10^{-6} mol·cm^{-3}).

ORR accelerated durability tests (ADTs) were conducted in O_2-saturated 0.1 M KOH solution within 0.5 to 1.0 V potential range at a sweep rate of 100 mV·s^{-1} for up to 10,000 cycles. Then the ORR activity was measured in a fresh electrolyte under the same conditions as the above ORR measurements.

Part II: Figures and tables

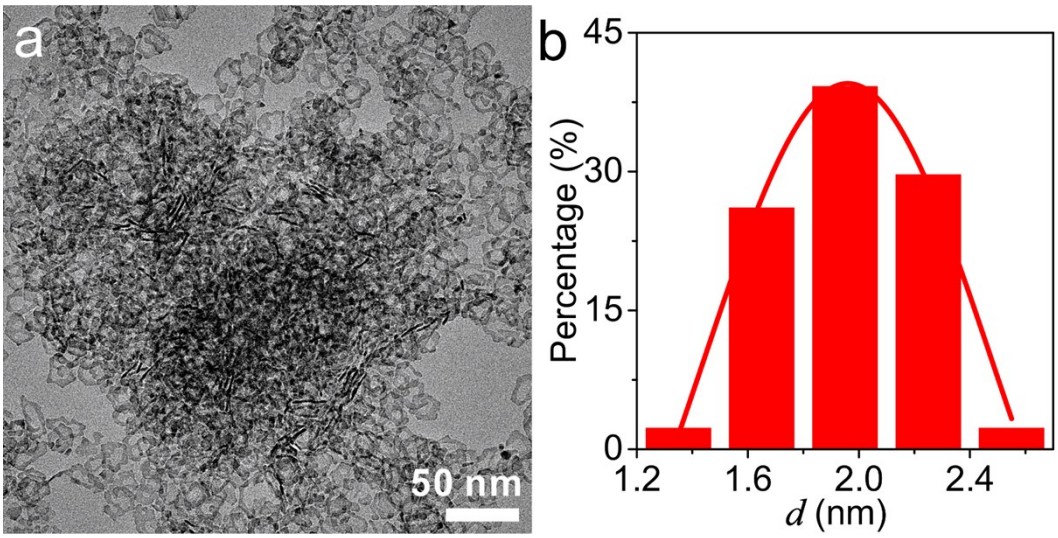

Fig. S1 (a) TEM image of $Pd_{55}Pt_{18}Co_{27}$ NRs; (b) corresponding statics for the average thickness (*d*) of $Pd_{55}Pt_{18}Co_{27}$ NRs.

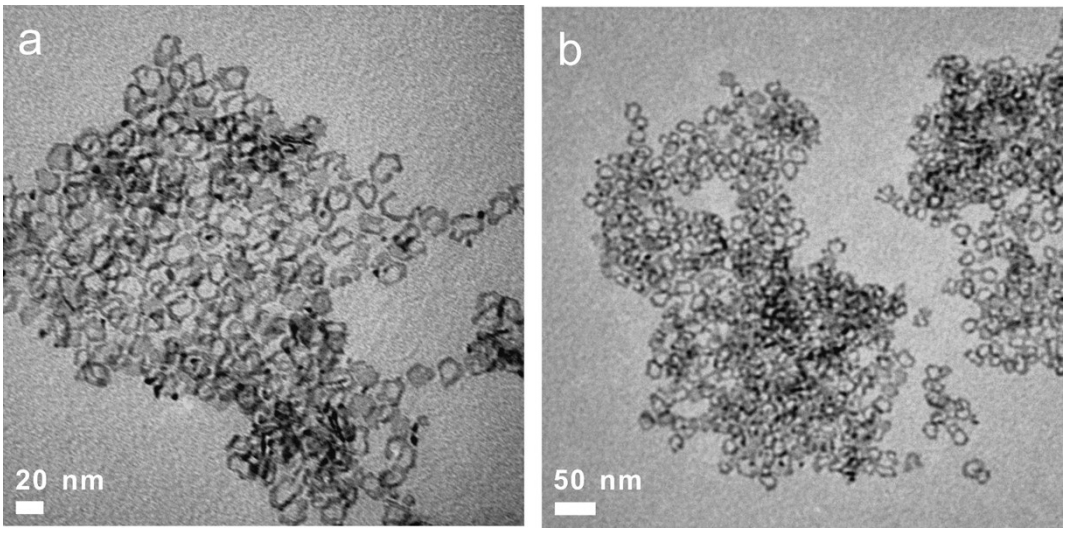

Fig. S2 TEM images of $Pd_{58}Pt_{15}Ni_{27}$ NRs synthesized according to the standard procedure by replacing the $Co(acac)_2$ with 30.8 mg $Ni(acac)_2$. The atomic ratio was determined by ICP-MS.

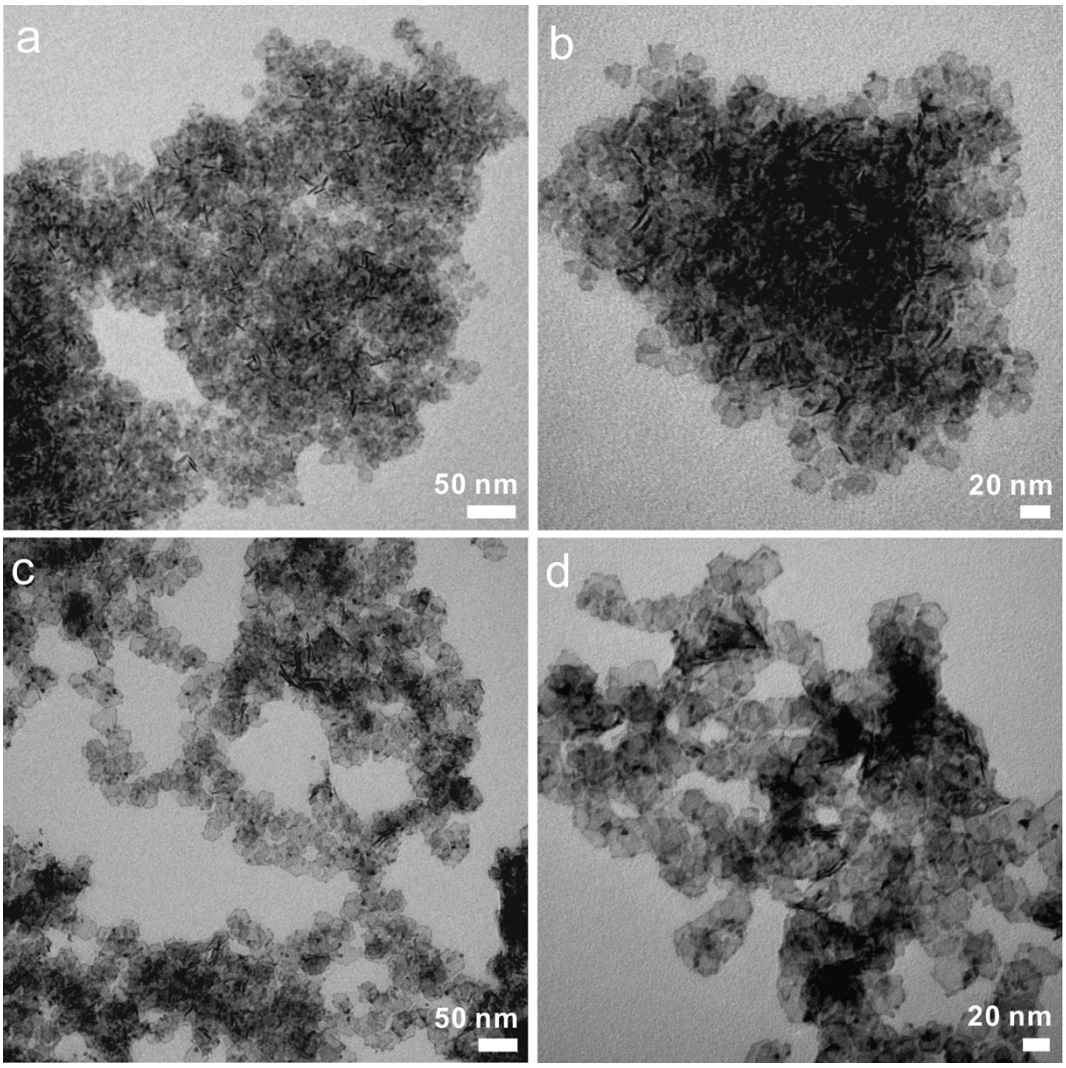

Fig. S3 TEM images of (a, b) $Pd_{63}Pt_{16}Co_{21}$ and (c, d) $Pd_{74}Pt_{26}$ NSs.

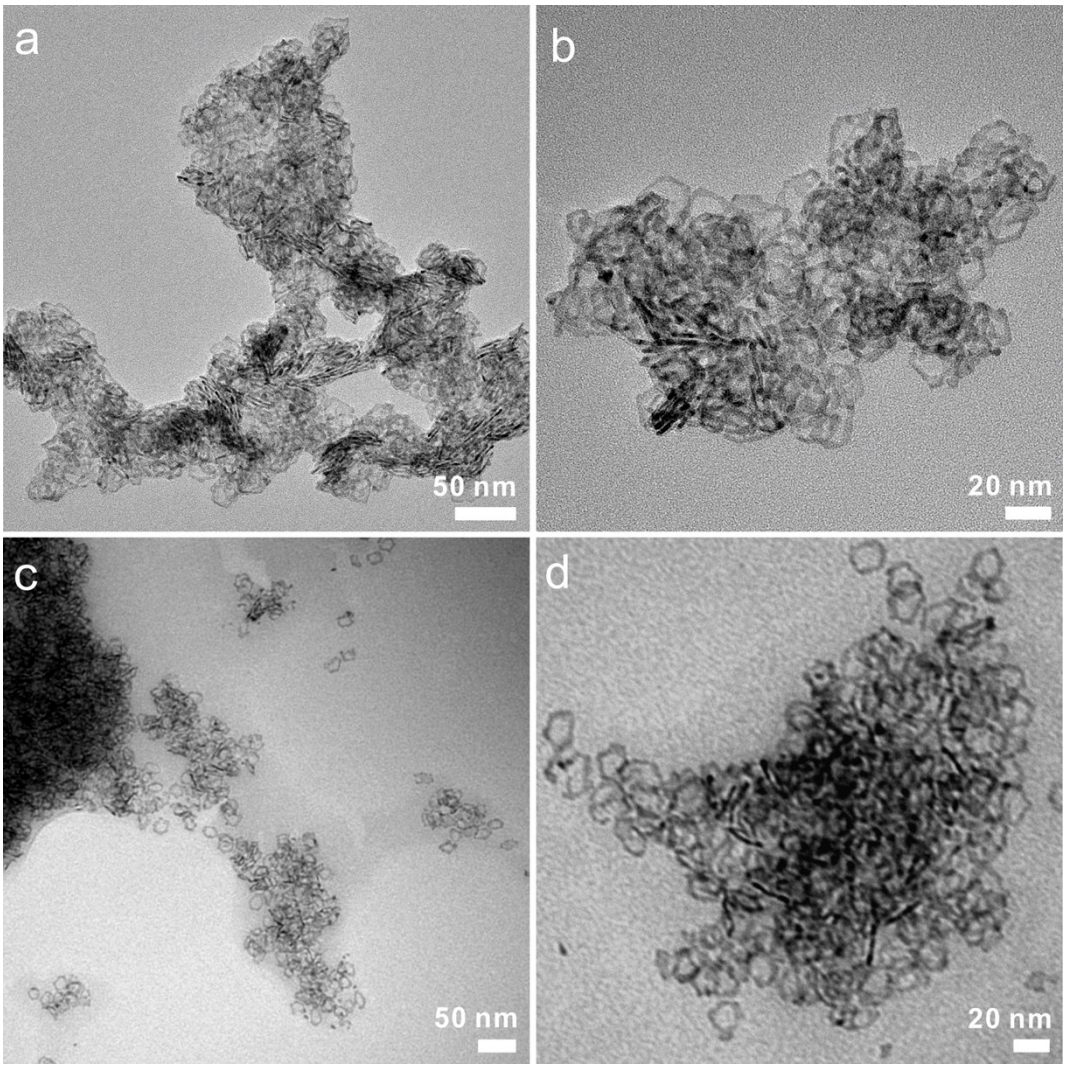

Fig. S4 TEM images of (a, b) $Pd_{76}Pt_{19}Co_5$ and (c, d) $Pd_{37}Pt_{10}Co_{53}$ NRs.

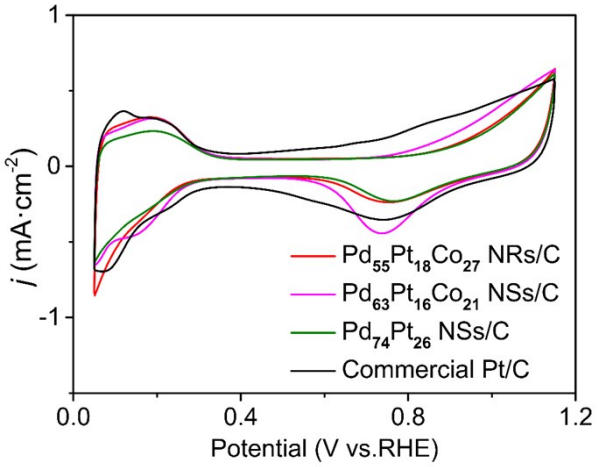

Fig. S5 Cyclic voltammograms (CVs) of $Pd_{55}Pt_{18}Co_{27}$ NRs/C, $Pd_{63}Pt_{16}Co_{21}$ NSs/C, $Pd_{74}Pt_{26}$ NSs/C and commercial Pt/C recorded in N_2-saturated 0.1 M $HClO_4$ solution.

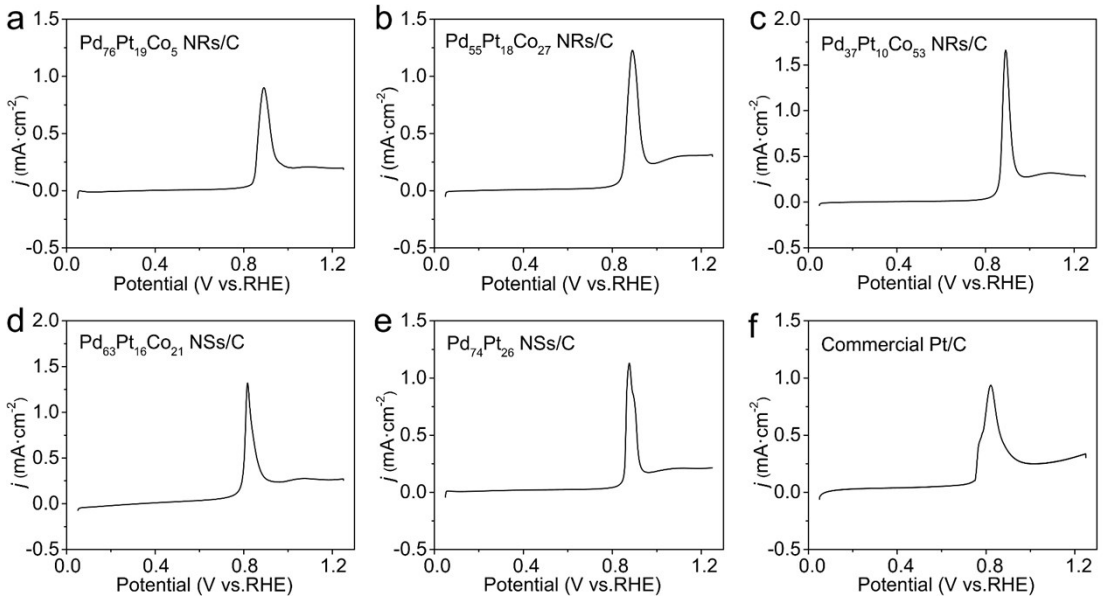

Fig. S6 CO stripping voltammograms of (a) $Pd_{76}Pt_{19}Co_5$ NRs/C, (b) $Pd_{55}Pt_{18}Co_{27}$ NRs/C, (c) $Pd_{37}Pt_{10}Co_{53}$ NRs/C, (d) $Pd_{63}Pt_{16}Co_{21}$ NSs/C, (e) $Pd_{74}Pt_{26}$ NSs/C, (f) and commercial Pt/C performed in the N_2-saturated 0.1 M $HClO_4$ solution.

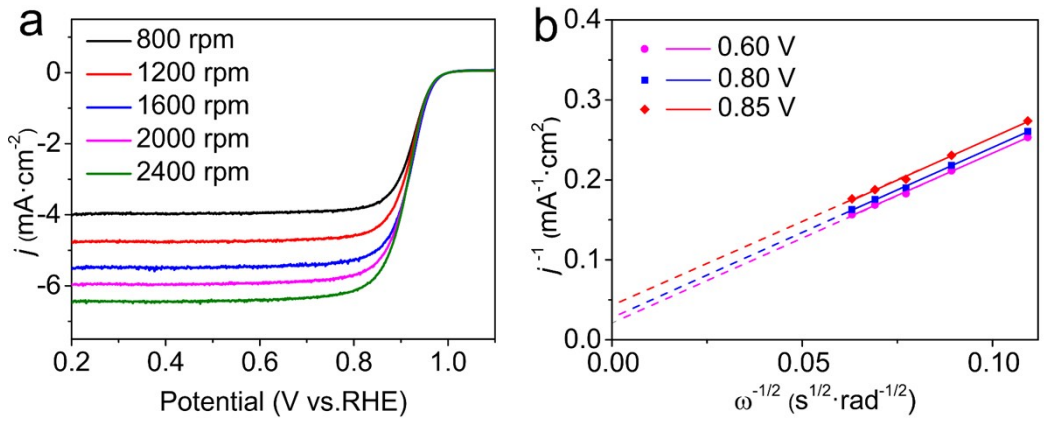

Fig. S7 (a) ORR polarization curves of $Pd_{76}Pt_{19}Co_5$ NRs/C with different rotating rates at 10 $mV \cdot s^{-1}$, (b) the Koutecký-Levich (K-L) fittings acquired at different potentials.

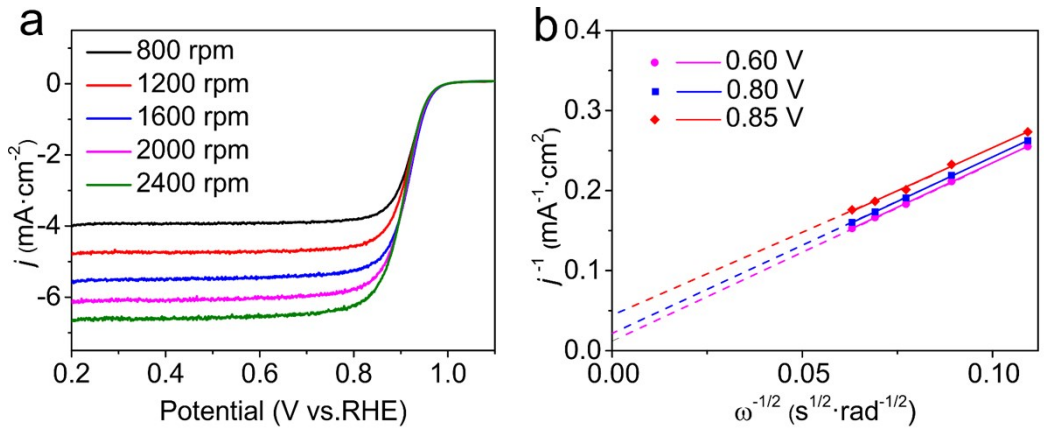

Fig. S8 (a) ORR polarization curves of $Pd_{37}Pt_{10}Co_{53}$ NRs/C with different rotating rates at 10 $mV \cdot s^{-1}$, (b) the Koutecký-Levich (K-L) fittings acquired at different potentials.

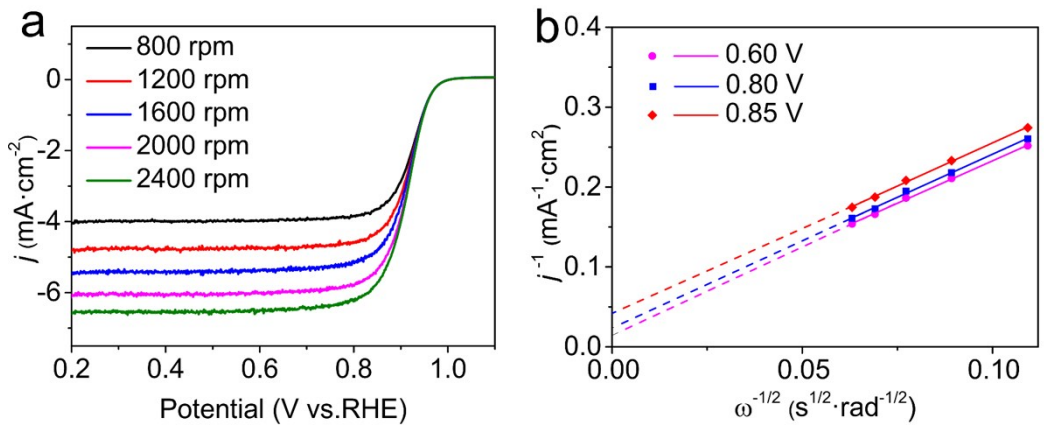

Fig. S9 (a) ORR polarization curves of $Pd_{63}Pt_{16}Co_{21}$ NSs/C with different rotating rates at 10 $mV \cdot s^{-1}$, (b) the Koutecký-Levich (K-L) fittings acquired at different potentials.

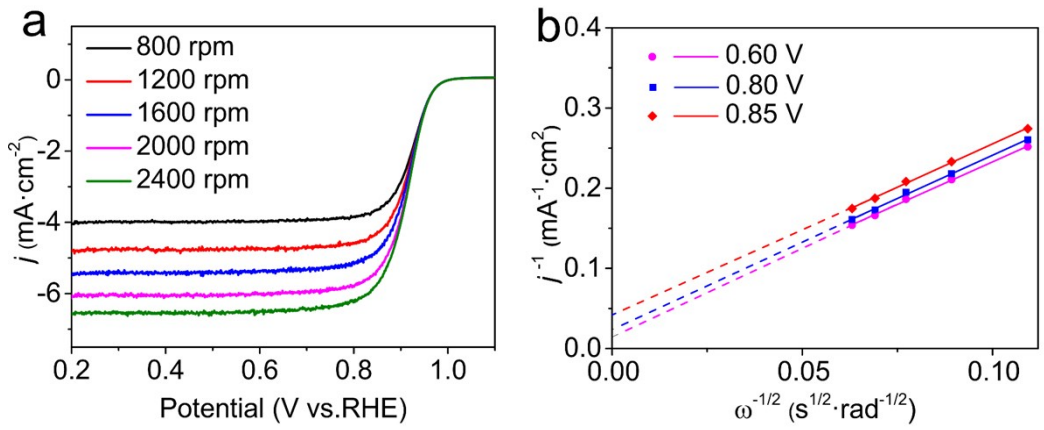

Fig. S10 (a) ORR polarization curves of $Pd_{74}Pt_{26}$ NSs/C with different rotating rates at 10 $mV \cdot s^{-1}$, (b) the Koutecký-Levich (K-L) fittings acquired at different potentials.

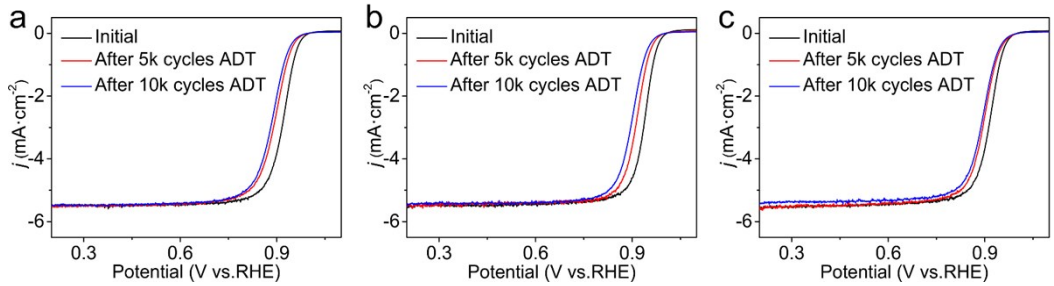

Fig. S11 Long-term ORR accelerated durability tests (ADTs) of (a) $Pd_{76}Pt_{19}Co_5$ NRs/C, (b) $Pd_{55}Pt_{18}Co_{27}$ NRs/C and (c) $Pd_{37}Pt_{10}Co_{53}$ NRs/C.

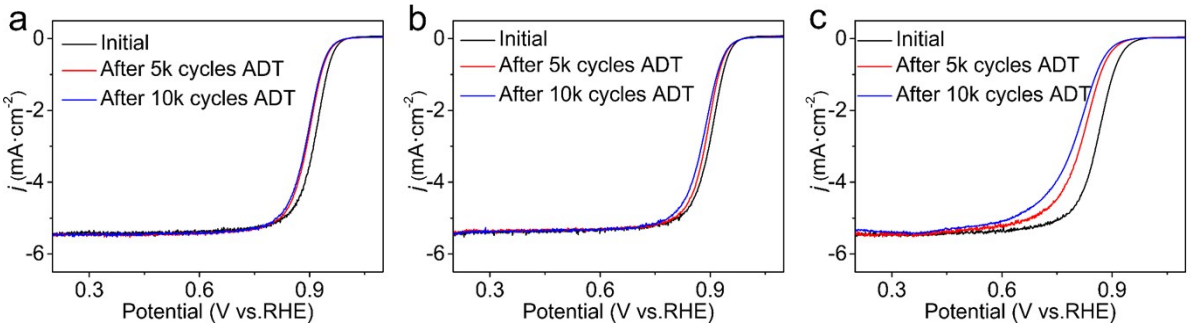

Fig. S12 Long-term ORR accelerated durability tests (ADTs) of (a) $Pd_{63}Pt_{16}Co_{21}$ NSs/C, (b) $Pd_{74}Pt_{26}$ NSs/C and (c) commercial Pt/C.

Table S1. The ORR electron transfer numbers (n) and kinetic current densities (j_k) of $Pd_{76}Pt_{19}Co_5$ NRs/C, $Pd_{55}Pt_{18}Co_{27}$ NRs/C, $Pd_{37}Pt_{10}Co_{53}$ NRs/C, $Pd_{63}Pt_{16}Co_{21}$ NSs/C and $Pd_{74}Pt_{26}$ NSs/C attained from the linear fitting of Koutecký-Levich (K-L) equation at different potentials.

Electrode	E (V vs RHE)	n	j_k (mA·cm^{-2})
$Pd_{76}Pt_{19}Co_5$ NRs/C	0.60	4.03	45.45
	0.80	4.01	35.71
	0.85	3.99	25.00
$Pd_{55}Pt_{18}Co_{27}$ NRs/C	0.60	3.83	83.33
	0.80	3.80	66.67
	0.85	3.80	47.62
$Pd_{37}Pt_{10}Co_{53}$ NRs/C	0.60	3.84	76.92
	0.80	3.84	50.00
	0.85	3.96	26.31
$Pd_{63}Pt_{16}Co_{21}$ NSs/C	0.60	4.01	50.00
	0.80	3.95	40.00
	0.85	3.94	25.64
$Pd_{76}Pt_{24}$ NSs/C	0.60	3.84	71.43
	0.80	3.81	40.00
	0.85	3.80	17.86

Table S2. ORR mass activity of $Pd_{76}Pt_{19}Co_5$ NRs/C, $Pd_{55}Pt_{18}Co_{27}$ NRs/C, $Pd_{37}Pt_{10}Co_{53}$ NRs/C, $Pd_{63}Pt_{16}Co_{21}$ NSs/C, $Pd_{74}Pt_{26}$ NSs/C, and commercial Pt/C in the long-term ORR accelerated durability tests.

Electrode	ADT cycles	j_m ($A \cdot mg^{-1}_{Pt+Pd}$)
$Pd_{76}Pt_{19}Co_5$ NRs/C	1st	1.20
	5,000th	0.43
	10,000th	0.31
$Pd_{55}Pt_{18}Co_{27}$ NRs/C	1st	2.73
	5,000th	1.01
	10,000th	0.53
$Pd_{37}Pt_{10}Co_{53}$ NRs/C	1st	1.06
	5,000th	0.48
	10,000th	0.40
$Pd_{63}Pt_{16}Co_{21}$ NSs/C	1st	0.99
	5,000th	0.47
	10,000th	0.41
$Pd_{76}Pt_{24}$ NSs/C	1st	0.57
	5,000th	0.35
	10,000th	0.26
Commercial Pt/C	1st	0.13
	5,000th	0.04
	10,000th	0.03

Note 1. Calculation method for the edge ratios of 2D PdPtCo NRs and NSs.

To estimate the edge ratios of NRs, we assumed the regular hexagonal prism with concentric hexagonal hole in the central area as the approximate simple model of the synthesized 2D multimetallic PdPtCo ultrathin NR (Fig. S13(a)). According to the corresponding edge length (*l* nm), width (*w* nm), and thickness (*d* nm), the edge ratio of the NRs can be calculated as shown below.

The surface area of top/bottom faces:

$$A_{surface} = 2 \times 6 \times \frac{1}{2} \times \frac{\sqrt{3}}{2} \times [l^2 - (l - w)^2]$$

The surface area of edges:

$$A_{edge} = 6 \times [l + (l - w)] \times d$$

The average edge ratio ($ER\%$) of NRs:

$$ER\% = \frac{A_{edge}}{A_{surface} + A_{edge}} \times 100\%$$

Similarly, $ER\%$ of NSs can be calculated accordingly by changing to the corresponding $A_{surface}^{'}$ and $A_{edge}^{'}$ of NSs (Fig. S13(b)).

The surface area of top/bottom faces:

$$A_{surface}^{'} = 2 \times 6 \times \frac{1}{2} \times \frac{\sqrt{3}}{2} \times l^2$$

The surface area of edges:

$$A_{edge}^{'} = 6 \times l \times d$$

Here, the structural parameters and calculated edge ratios of $Pd_{55}Pt_{18}Co_{27}$ NRs, $Pd_{63}Pt_{16}Co_{21}$ NSs and $Pd_{74}Pt_{26}$ NSs are shown below.

2D multimetallic NRs and NSs	***l* (nm)**	***w* (nm)**	***d* (nm)**	***ER*%**
$Pd_{55}Pt_{18}Co_{27}$ NRs	10.13	2.75	1.96	45.14%
$Pd_{63}Pt_{16}Co_{21}$ NSs	7.90	N.A.	1.72	20.09%
$Pd_{74}Pt_{26}$ NSs	13.91	N.A.	1.50	11.08%

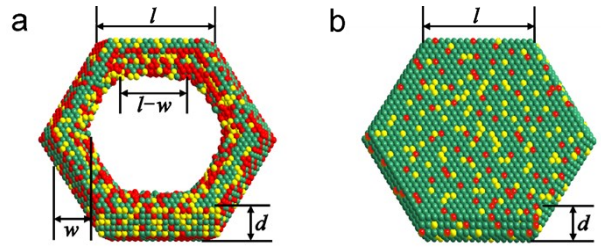

Fig. S13 Atomical model of the synthesized 2D multimetallic PdPtCo ultrathin NR (a) and NS (b).